Supporting Information

for *Adv. Mater. Interfaces,* DOI: 10.1002/admi.201800667

Patterned Nanobrush Nature Mimics with Unprecedented Water-Harvesting Efficiency

*Depanjan Sarkar, Anindita Mahapatra, Anirban Som, Ramesh Kumar, Ankit Nagar, Avijit Baidya, and Thalappil Pradeep**

Supporting Information

Patterned Nanobrush Nature Mimics with Unprecedented Water Harvesting Efficiency

*Depanjan Sarkar, Anindita Mahapatra, Anirban Som, Ramesh Kumar, Ankit Nagar, Avijit Baidya and Thalappil Pradeep**

Synthesis and characterization of Ag NWs

For electrospray deposition, a homemade nanoelectrospray (nESI) source was made by pulling a borosilicate glass capillary (0.86 mm inner diameter, 1.5 mm outer diameter, and 10 cm length) into two. The pulling was performed in a controlled fashion in order to achieve an inner diameter of approximately 15 µm at the tip. These tips were used as nESI sources in all our deposition experiments. For the elrctrospray process, a nESI tip was filled with a 10 mM aqueous solution of silver acetate (AgOAc) using a micro injector and a potential in the range of 2-2.5 kV was applied to it through a platinum wire (0.1 mm diameter, Sigma Aldrich) electrode. In all the experiments, the home-built nanoelectrospray (nESI) source was used to deliver charged droplets of aqueous AgOAc solution onto a conductive stainless steel wire mesh placed on top of an indium tin oxide (ITO) coated glass collector. In case of transmission electron microscopy (TEM) measurement, the droplets were collected on an empty (without carbon coating) TEM grid. The wire mesh or the empty TEM grid acts as a static mask between the ITO slide and the spray plume. The ITO slide was grounded through a picoammeter to measure the deposition current. Pt wire was used as an electrode due to its inert nature towards other reagents. A plume of charged droplets containing solvated silver ions like $Ag(H_2O)^+$ and $Ag(H_2O)_2^+$ was ejected from the nESI tip, as confirmed by mass spectrometry. Figure S1 shows a schematic representation of the experimental set up with dimensional details. Figure S2 show a mass spectrum collected from electrospray of AgOAc solution.

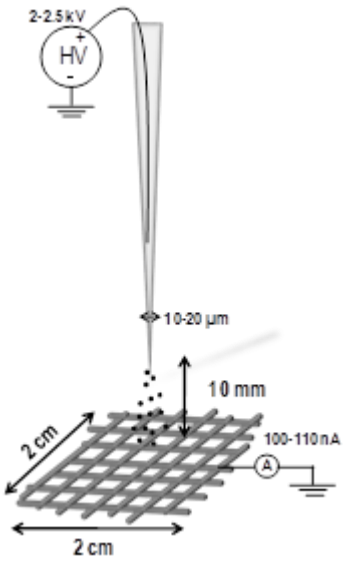

Figure S1. Schematic representation of the ESD set up. Representation of the dimensional details.

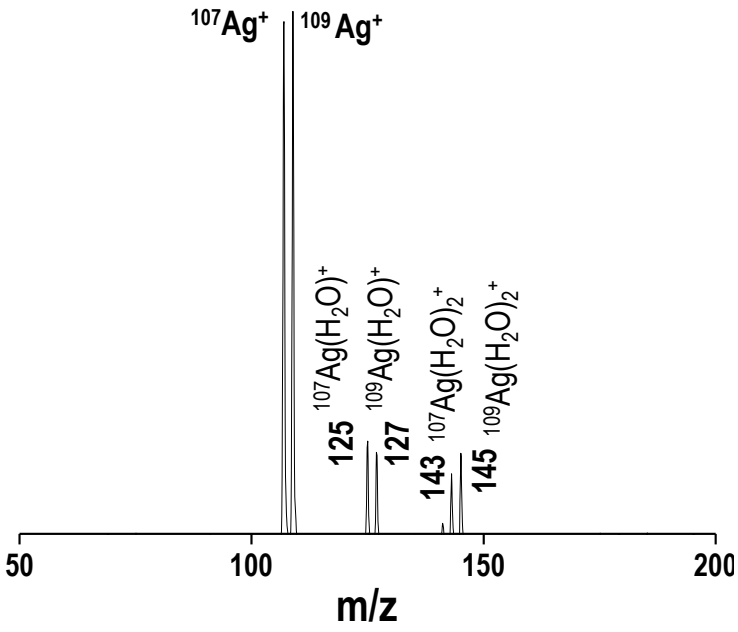

Figure S2. Mass spectrum collected from an aqueous solution of Ag(OAc).

In the course of electrospray deposition, a black circular spot (typical diameter 2-5 mm depending on the distance between the nESI tip and the collector) due to the incoming spray plume appeared on the mask (SS wire mesh/empty TEM grid) itself. These were taken for further characterization. Deposition time can be varied to control the sizes of the NWs. For our experiments we have used NWs made by 6h deposition at a rate of 100-110 nA deposition current.

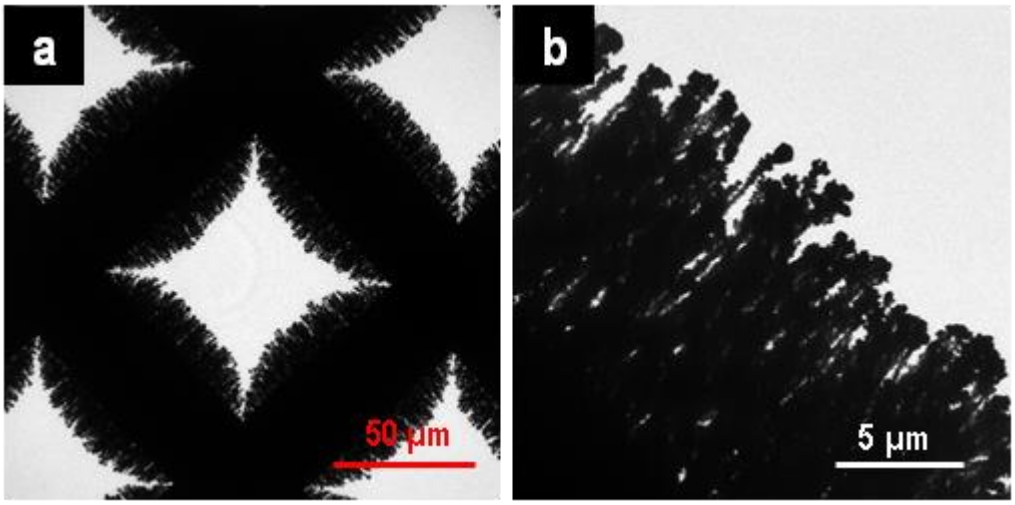

Figure S3. TEM images of as-synthesized Ag NWs. TEM images of it at different magnifications.

Electron microscopy imaging was peformed to understand the black spot on the mask. TEM imaging of the grid revealed an unusual brush-like growth of nanowires, with a head on stacking of bare Ag NPs comprising each nanowire. Figure S3a and b show TEM images of such nanowires at different magnifications. The higher magnification image in Figure S3b clearly shows that the Ag nanobrushes have a linear morphology, some of them somewhat

bent. The growth in each Ag NW is shown to be one-dimensional and not dendritic although the electron beam induced adhesion of the wires is possible; they are clearly not branched. These brush-like growth was only seen on the mask. On the other hand, the ITO collector below the mask collected Ag NPs. Figure S4a and b show TEM images of the Ag NPs formed on the collector while deposition. In this case, a carbon coated TEM grid was used as the collector instead of an ITO slide.

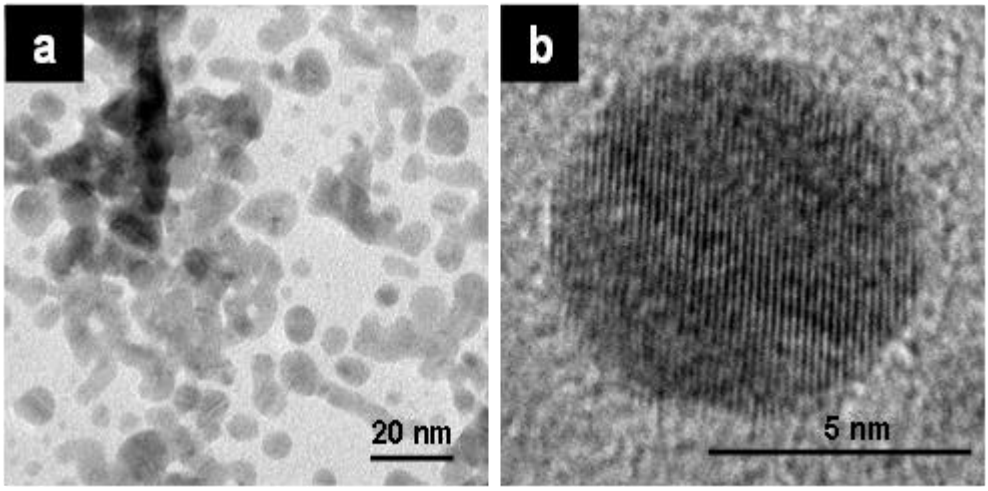

Figure S4. TEM images of Ag NPs. a) and b) TEM images of Ag NPs formed on the collector during electrospray deposition.

Detailed investigation revealed that the Ag NWs are typically assembled in small groups (nanobristles) and these in turn are arranged on the surface to create a nanobrush. A single nanobristle is actually a braid of several NWs which in turn possesses pearl-necklace type morphology. Figure S5a shows a TEM image of a nanobristle of the synthesized nanobrushes. From the image it is clearly seen that each bristle is a braid of several thinner nanowires. Figure S5b shows higher magnification TEM image taken from a single NW. Head on arrangement of the Ag NPs leading to pearl-necklace morphology is clearly seen.

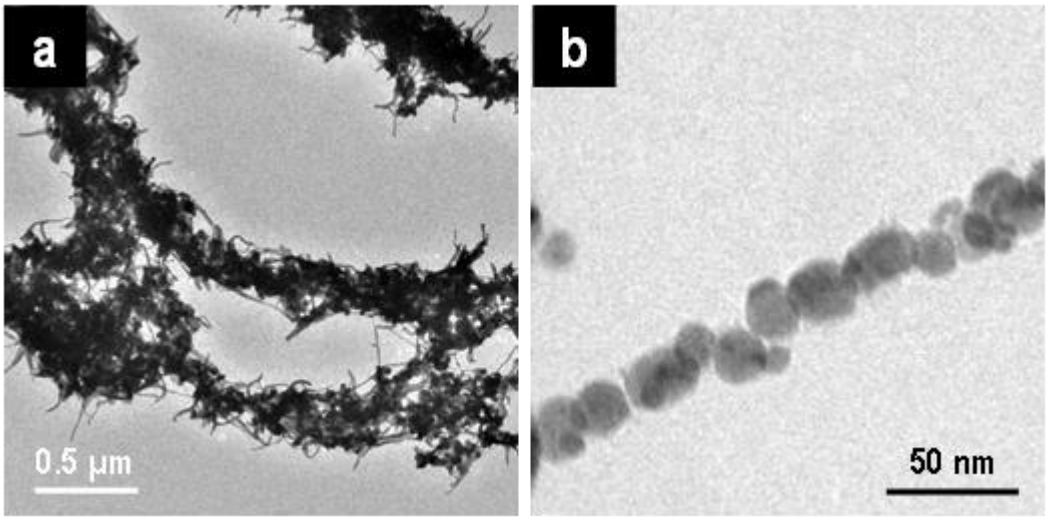

Figure S5. TEM images of a single NW. a) single bristle of the Ag nanobrush, b) single building block of a bristle showing pearl-necklace type morphology.

The above data prove that the deposition of solvated metal ions results in neutralization, aggregation and orientation to form 1D nanostructures.

Careful investigation of the TEM data tell us further interesting facts. A TEM image of a single square of the empty TEM grid (Figure S6a) shows uniform assembly of bristles protruding out from the edges. The bristles appear apparently continuous in low magnification (Figure S6a), but upon closer inspection, they have a rough surface beacuse of the braiding of invidual NWs (Figure S6b). Figure S7 shows a high resolution transmission electron microscopy (HRTEM) image from the tip of a NW showing crystalline NPs in the NWs. The measured Ag (111) lattice spacing and energy dispersive sectroscopy (EDS) (Figure S8) confirm the presence of crystalline AgNPs.

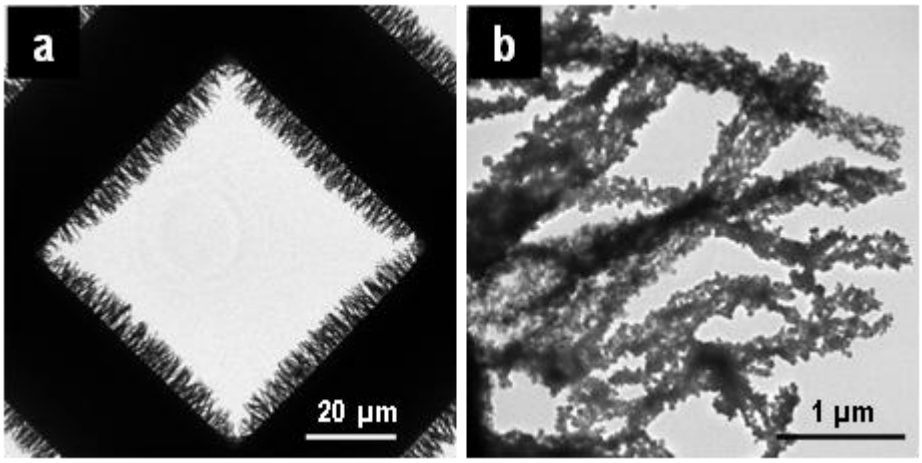

Figure S6. One dimensional nature of the Ag NWs. a) TEM image of a single square of an empty TEM grid, b) higher magnification image of the nanobristles showing the surface roughness.

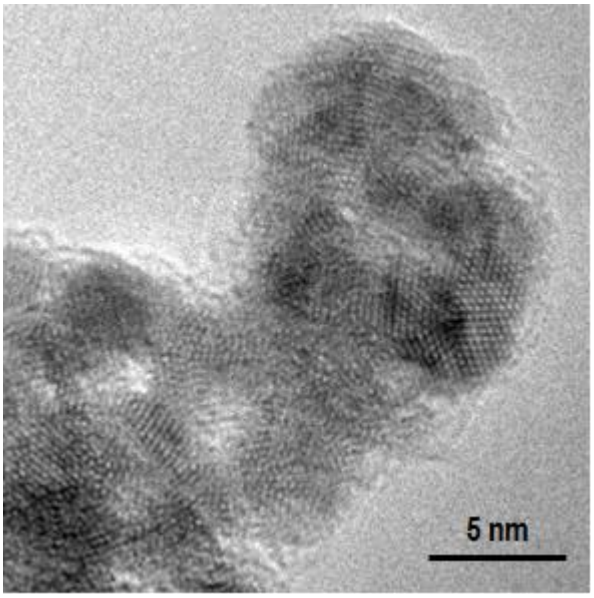

Figure S7. Crystallinity of the Ag NPs. High resolution transmission electron microscopy (HRTEM) image of a tip of a nanobristle showing the presence of crystalline Ag NPs.

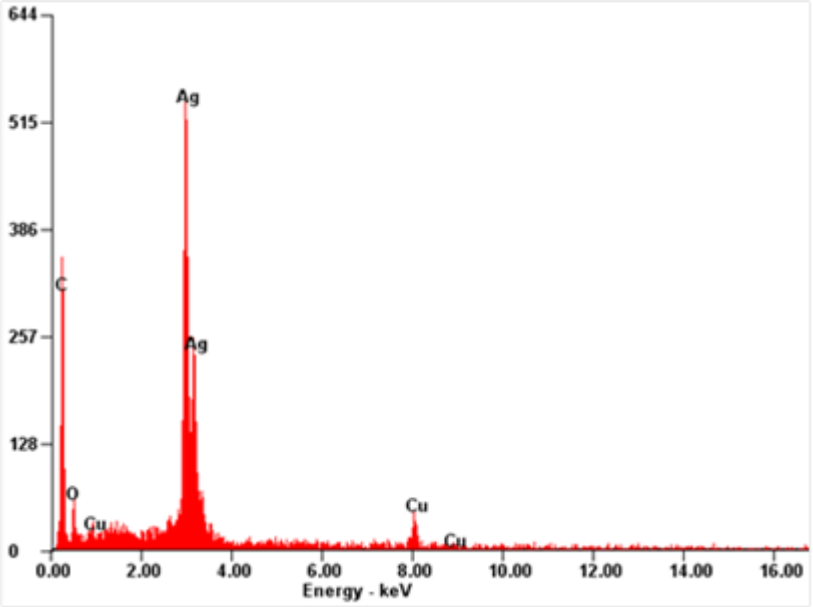

Figure S8. Elemental analyusis. SEM EDS spectrum collected from the Ag nanobrushes.

TEM images may imply that the NW structures are formed only at the edges of the square apertures of the mesh. But that is not the case. For better understanding of the nanobrush growth, SEM analysis was performed on the circular spot (~1.5-2.5 mm in diameter, depending upon the distance of the collector surface from the spray emitter) on the mask. Figure S9a and b show SEM images taken for Ag nanobrushes grown on an empty TEM grid and a SS wire mesh, respectively.

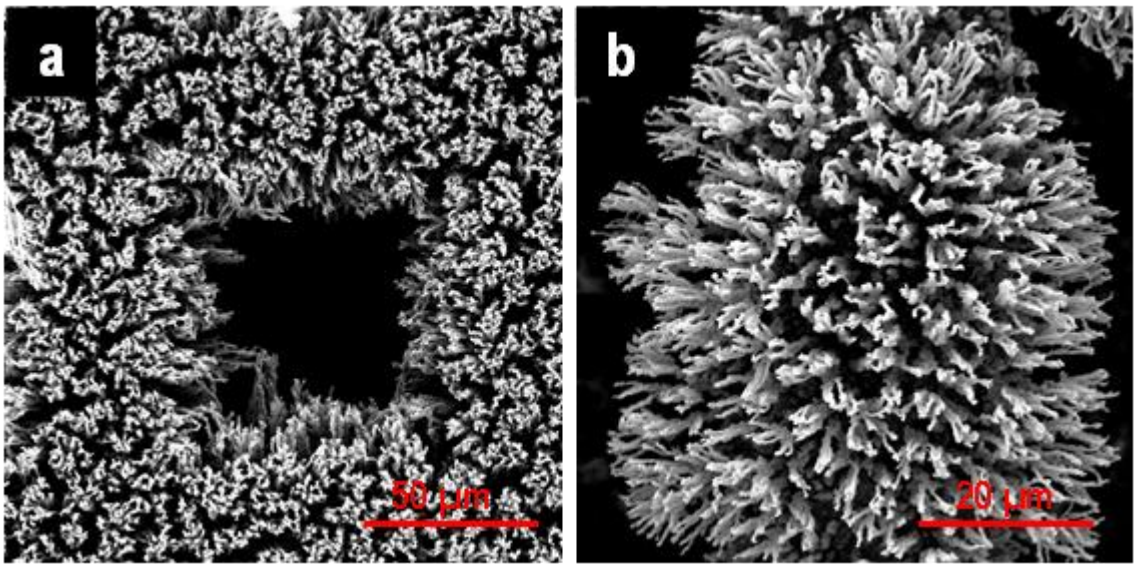

Figure S9. SEM images of the as-synthesized Ag NWs. SEM image of it grown on a) empty TEM grid, b) SS wire mesh.

SEM images show that the growth of the Ag nanobrushes are extended all over the grid/SS wire mesh providing a grassland like morphology. Conducting mesh is essential for the

growth. Control experiments were performed to prove that the size and shape of the mesh do not effect the growth. On the other hand, a conducting mesh as mask is the essential criteria for the NWs growth.

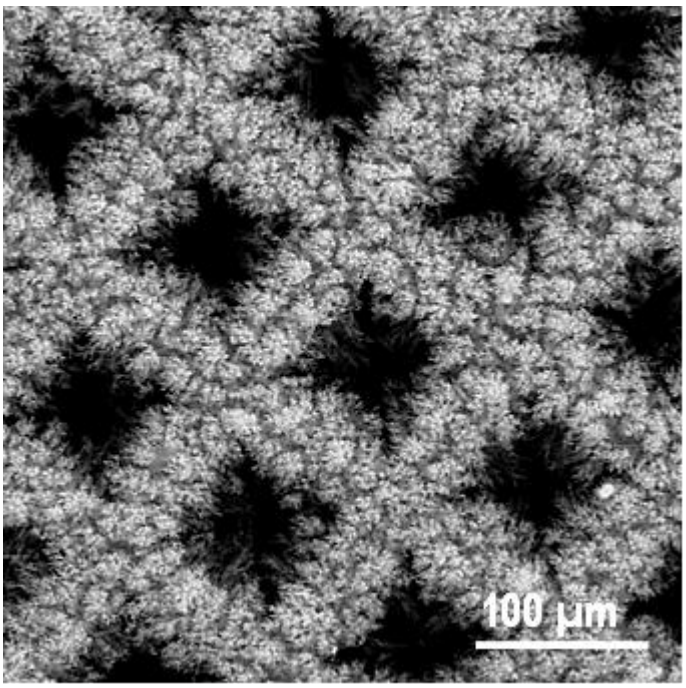

Figure S10. Large area image. SEM image of the AgNWs grown over a large area.

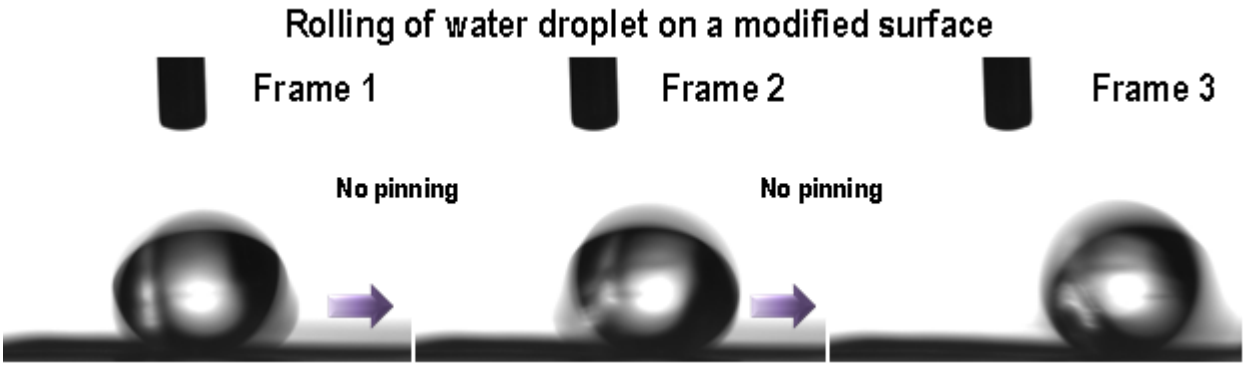

Figure S11. Droplet pinning experiment. Images of a water droplet rolling on the FT-coated Ag brushes. No pinning of the droplet was observed, proving the superhydrophobicity of the surface.

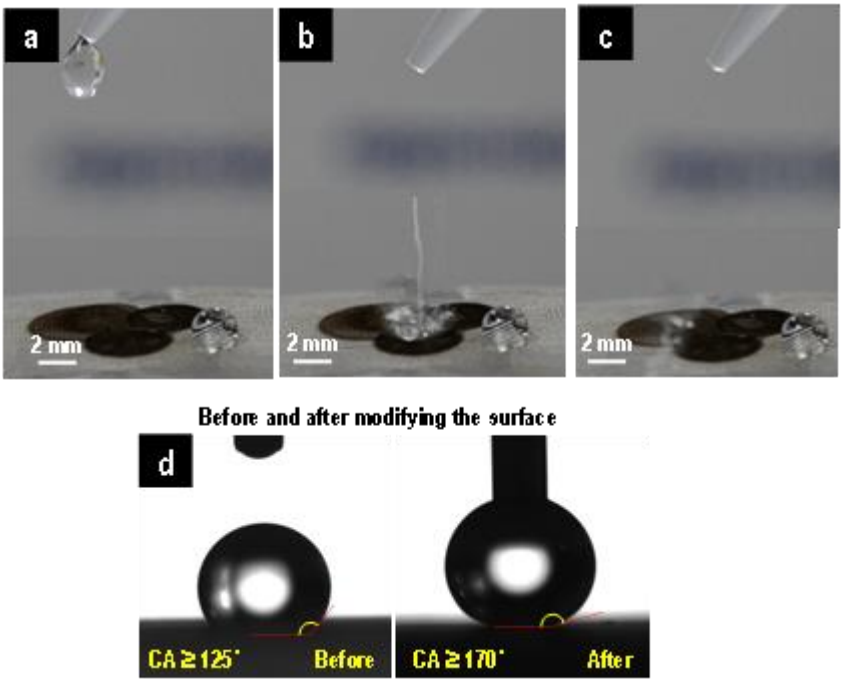

Figure S12. Proof of superhydrophobicity. a-c) Optical images of a water droplet bouncing off from the FT coated Ag brush substrate while another water droplet is stranded on the bare stainless steel wire mesh. d) Contact angle measurement on the superhydrophobic Ag nanobrushes.

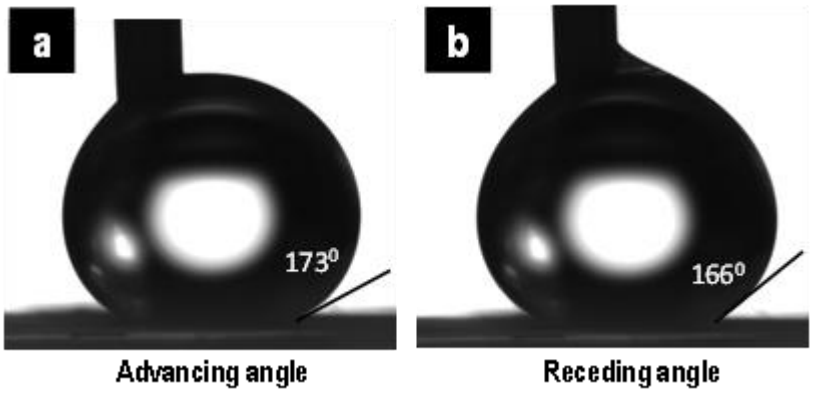

Figure S13. Advancing and receding angle. Measurement of a) advancement and b) receding contact angle of a water droplet on the superhydrophobic nanobrushes. The drop had to be held by touching it with a pipette tip.

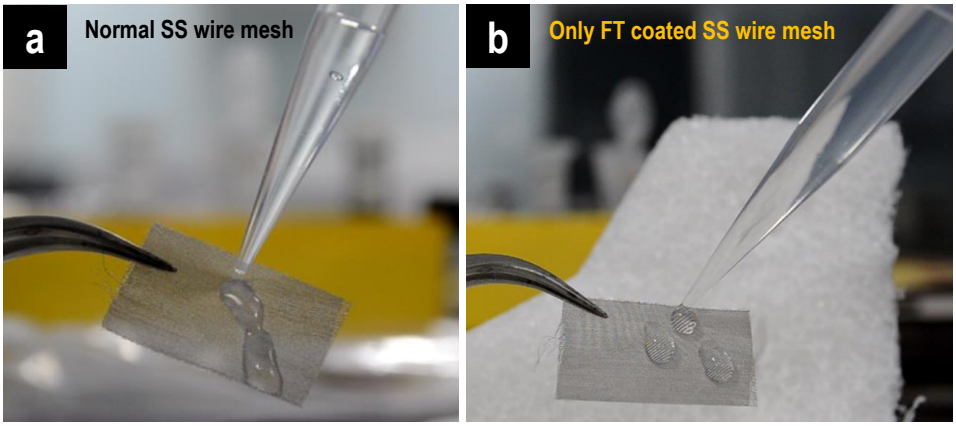

Figure S14. Control experiments. a) Optical image of water droplets on normal SS wire mesh, b) optical image of water droplet sticking on a FT-coated SS wire mesh. Here also the droplets did not bounce off and got stuck to the surface. However, when it was sprayed with FT, the stainless steel mesh surface became hydrophobic to some extent.

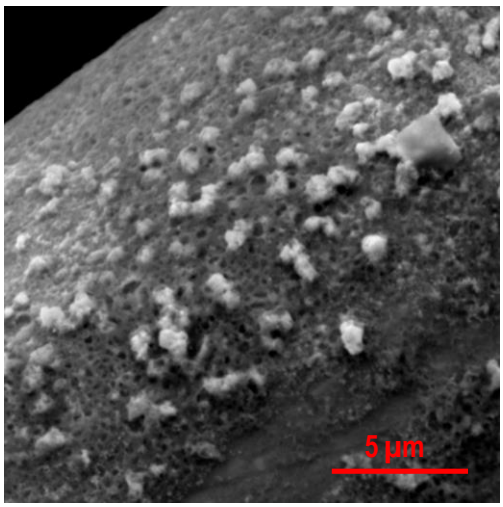

Figure S15. Control experiment. SEM image showing that the morphology of the Ag NWs was destroyed after spray coating of FT with a commercial sprayer.

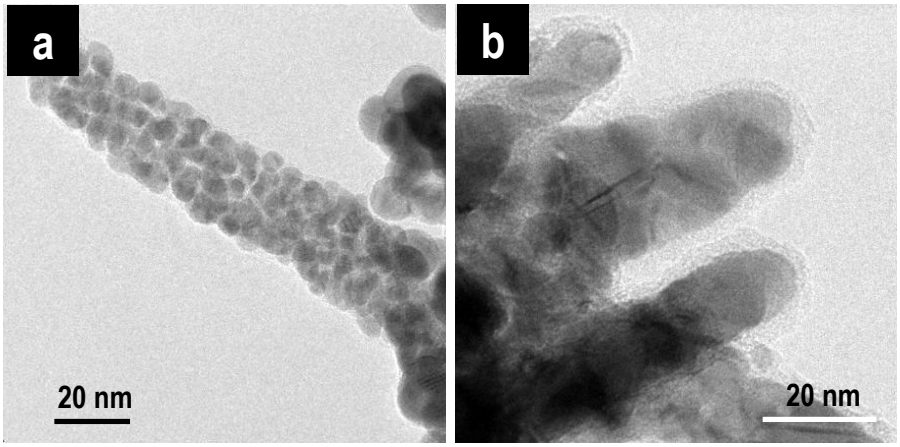

Figure S16. TEM images of the surface modified Ag NWs. TEM images of the Ag NWs a) before and b) after FT coating on the Ag NWs.

Proof of superhydrophobicity: To confirm the surface energy of the modified surface, the wettability was studied with static and dynamic contact angle measurements. The surface energy of the FT modified Ag nanobrushes is so low that water droplet did not stick on to it. The water droplets rolls off (no pinning) easily (Figure S11). To understand the wetting property in detail, contact angle hysteresis (CAH) was measured through dynamic CA experiment and shown in Figure S13. Static contact angle (CA) of water drop was measured before and after the experiment to check the change in wettability of the surface. For both the cases, CA was observed to be greater than 170 ° (Figure S19 c and d). This can relate with the stability and durability of the modified brushes.

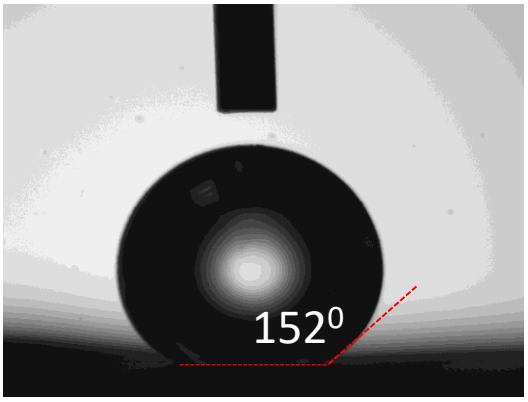

Figure S17. Contact angle measurement after the creation of hydrophilic zones over the super hydrophobic NWs.

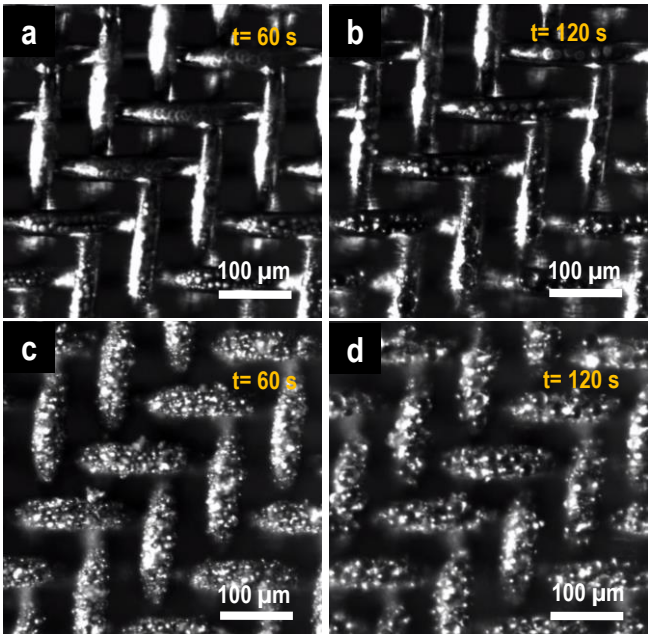

Figure S18. Optical microscopic images of water droplet condensed on the surface. a) and b) Optical images of a normal stainless steel wire mesh after 60 and 120 seconds of cooling, respectively. Condensation of water droplets was seen on the wire mesh. c) and d) Optical images of condensation of water on the stainless steel wire mesh containing superhydrophobic Ag nanobrush with hydrophilic protrusions. It is seen that the amount of water captured in this case is much larger in comparison to the normal wire mesh.

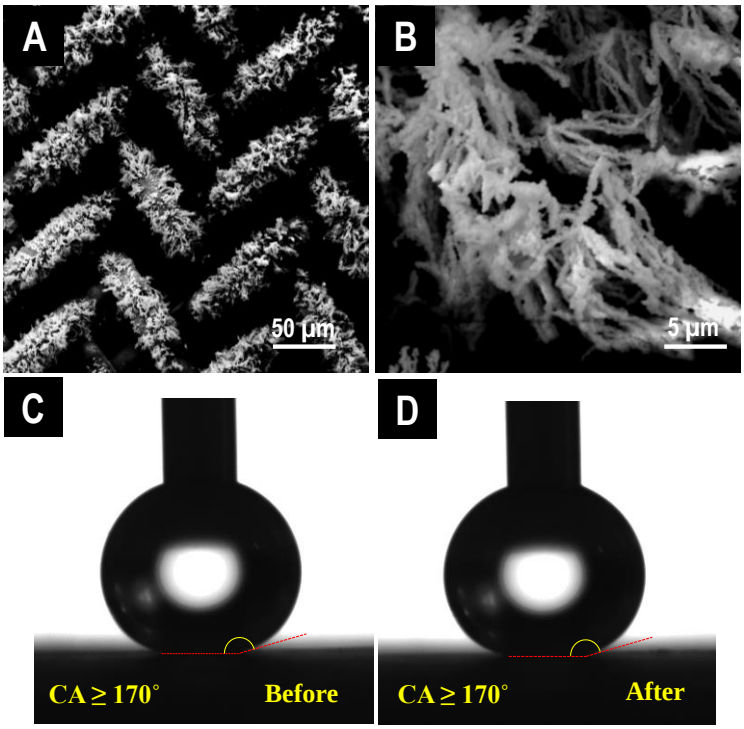

Figure S19. Test of stability of the surface. a) and b) SEM images of the superhydrophobic brushes after 5 cycles of water capture experiment, showing the morphology is intact, c) and d) contact angle of a water droplet on the same showing that the superhydrophobic nature of the surface is largely unchanged during the water capture experiments.

Video S1**.** Atmospheric water capture by the hydrophilic-hydrophobic patterned NWs under an optical microscope.

Video S2. Atmospheric water capture on a hydrophilic-hydrophobic patterned area (4 cm^2) using our prototype. The white spots seen in the video are due to the residue of the silver paste used for contact between the surface and the Peltier cooler. In subsequent experiments, we changed this to carbon take for better water transport.